A flexible and unified framework for single- and multi-outcome Mendelian randomization using summary statistics

Authors

Bowei Kang, David Li, Ke Xu, ...,
Brandon L. Pierce, David A. Bennett, Lin S. Chen

Correspondence

lchen4@bsd.uchicago.edu

Mapping causal genes from molecular QTL data remains challenging due to limited instruments. Kang et al. introduce FusioMR, a Bayesian Mendelian randomization framework that leverages gene-region-specific information and supports multi-outcome analyses, improving causal inference for molecular traits and facilitating the discovery of disease risk genes.

Kang et al., 2026, The American Journal of Human Genetics *113*, 950–965
May 7, 2026
https://doi.org/10.1016/j.ajhg.2026.03.017

CellPress

ARTICLE

A flexible and unified framework for single- and multi-outcome Mendelian randomization using summary statistics

Bowei Kang,[1] David Li,[1] Ke Xu,[1,2] Jianhai Chen,[1] Sihao Feng,[1] Jinyu Wang,[3] Guimin Gao,[1] Shinya Tasaki,[4] Brandon L. Pierce,[1] David A. Bennett,[4] and Lin S. Chen[1,*]

Summary

Mendelian randomization (MR) is widely used to evaluate causal effects of complex trait exposures on disease outcomes. Recently, MR has been increasingly applied to molecular traits, such as gene expression, to map risk genes. However, transcriptome-wide MR (TWMR) faces unique challenges. The number of available *cis*-QTLs as instrumental variables (IVs) is often limited, and horizontal pleiotropy is pervasive, violating core MR assumptions and compromising inference validity. We introduce FusioMR, a robust MR framework tailored for molecular trait exposures while also applicable to complex trait exposures. Our single-outcome model, FusioMR$_s$, incorporates gene-region-specific empirical priors informed by the number and strength of QTLs, linkage disequilibrium, and effect size consistency. It uses sampling-based inference to improve robustness when instruments are limited. Our multi-outcome model, FusioMR$_m$, is motivated by the observation that many complex diseases have correlated diseases, subtypes, or comorbidities, which could be affected by shared or correlated exposures. FusioMR$_m$ jointly analyzes two correlated outcomes, leveraging shared IVs and pleiotropic effects of shared/correlated exposures to improve estimation precision and power, particularly for underpowered outcomes. We applied FusioMR$_s$ to identify cell-type-specific gene expression traits associated with Alzheimer disease using single-cell eQTL and GWAS summary data. We applied FusioMR$_m$ to detect alternative polyadenylation events affecting atrial fibrillation and ischemic stroke, and to estimate the causal effect of low-density lipoprotein on ischemic stroke in South Asian populations by borrowing information from European ancestry data. These applications highlight the generalizability of FusioMR for both molecular and complex trait exposures.

Introduction

Mendelian randomization (MR) assesses the causal effects of exposures on complex disease outcomes, using genetic variants as instrumental variables (IVs).[1–5] Two-sample MR uses as input the summary statistics from genome-wide association studies (GWASs) of exposure and outcome, and has been widely used to evaluate causal links between complex trait exposures and disease risks.[6–8] More recently, transcriptome-wide MR (TWMR) uses MR for detecting gene expression levels as exposures, treating *cis*-expression quantitative trait loci (eQTL) as IVs.[9,10] In addition to gene expression, MR has been applied to other molecular traits, such as protein levels,[11,12] metabolites,[13] alternative splicing,[14] and DNA methylation,[15] as exposures to identify molecular risk factors for complex diseases.

MR faces unique challenges when studying molecular trait exposures. First, most existing MR methods were developed for analyzing complex trait exposures (such as body mass index[16,17]), which often have many strongly and independently associated genetic variants serving as IVs. In contrast, for molecular trait exposures, the number of available IVs, typically *cis*-QTLs, is often limited. Moreover, these *cis*-QTLs are frequently in linkage disequilibrium (LD) and many may have weak effects. Second, horizontal pleiotropy is pervasive for molecular trait exposures, leading to core IV assumption[2] violations. Molecular QTLs may affect the outcome through *trans*-genes or genetic pathways unrelated to the exposure (uncorrelated horizontal pleiotropy, UHP) or may be associated with unmeasured confounders such as local genes or other *cis*-associated molecular traits, creating correlated horizontal pleiotropy (CHP). For example, recent studies reported that 21% of methylation QTLs (mQTLs) colocalize with at least one eQTL.[18] As a result, when multi-omic QTLs are selected as IVs, MR analyses could be biased if not all associated molecular traits are accounted for. Finally, QTL effects may vary across samples and cellular contexts. This variability can weaken the consistency of IV-to-exposure associations in two-sample MR, potentially compromising the validity of causal inference.

Most existing MR methods were developed to analyze complex traits (with large sample sizes) as exposures, and may be inadequate for addressing horizontal pleiotropy when applied to molecular traits, which often have smaller sample sizes and a limited set of weak, correlated, and potentially inconsistent IVs. For example, the causal estimate from IVW[4] is biased in the presence of horizontal pleiotropy. MR-Egger[19] accounts for UHP but does not

[1]Department of Public Health Sciences, The University of Chicago, Chicago, IL, USA; [2]Department of Applied and Computational Mathematics and Statistics, University of Notre Dame, Notre Dame, IN, USA; [3]Department of Biostatistics and Health Data Science, School of Public Health, University of Pittsburgh, Pittsburgh, PA, USA; [4]Rush Alzheimer's Disease Center, Rush University Medical Center, Chicago, IL, USA
*Correspondence: lchen4@bsd.uchicago.edu
https://doi.org/10.1016/j.ajhg.2026.03.017.

allow for CHP. MR-Mix,[20] MR-ContMix,[21] and CAUSE[22] build mixture models to distinguish valid IVs from invalid ones (i.e., variants with pleiotropic effects). With a limited number of instruments, the estimation of a mixture model can be unreliable. MR-CUE[23] allows all IVs to have UHP and some IVs have IV-specific CHP effects from multiple confounders. It also requires a large number of IVs for reliable estimation. cML[24] uses a constrained maximum likelihood-based method to identify invalid IVs and estimate the causal effect. When the sample size is small or there are many invalid IVs with only weak pleiotropic effects, the consistency in selecting invalid IVs may not be achieved, potentially resulting in overfitting and inadequate control of the false positive rate. A data-perturbation-based version of cML[24] has been proposed to better control the type I error rate in challenging situations. However, it increases the computational burden and still requires a moderately large number of IVs. Additionally, cML,[24] MR-Mix,[20] and MR-ContMix[21] assume IV plurality, which may be violated when pervasive horizontal pleiotropy exists. MR^2[25] was developed for jointly analyzing multiple correlated outcomes, where its key innovation is the modeling of residual correlation across outcomes. It is not designed for single-outcome analyses and does not explicitly model CHP. As a summary, existing methods proposed for complex trait exposures cannot adequately address the unique challenges in TWMR analysis, highlighting the need for more robust and tailored approaches. cisMR-cML[26] was recently proposed for analyzing molecular traits with limited IVs. It allows some SNPs to have UHP or CHP and leverages correlated *cis*-SNPs and SNPs strongly associated with the outcome to identify invalid instruments. The performance of the method partly relies on the availability of outcome-associated SNPs and can show some inflation when such SNPs are absent. As new TWMR-focused methods continue to emerge, each relying on different assumptions, complementary approaches are needed.

In this work, we propose FusioMR, a flexible unified framework for single- and multi-outcome Mendelian randomization. FusioMR is a set of MR models for estimating causal effects of either molecular or complex trait exposures on one or more outcomes. It is built on a Bayesian hierarchical model and uses Gibbs sampling for estimation. In TWMR analyses with a limited number of *cis*-QTLs as IVs, we propose to construct priors based on gene-region-specific characteristics, such as the number and strength of QTLs, LD among selected IVs, and the joint distribution of QTL and GWAS effect sizes among IVs, to better capture gene-region-specific variability. The combination of sampling-based inference and region-specific priors improves the robustness and efficiency of the model estimation, especially in settings with limited or weak IVs. FusioMR allows all IVs to have UHP effects and some to have CHP effects. In TWMR analysis, FusioMR adopts a UHP-only model as default, with the option to estimate CHP effects when needed. The FusioMR$_s$ model assesses the causal effect of an exposure on a single outcome. FusioMR$_m$ builds a multi-outcome MR model, leveraging shared information among correlated exposures and correlated outcomes. By imposing correlated priors to model dependency among correlated exposures and among IVs associated with potential confounders for correlated outcomes, FusioMR$_m$ enhances the identification of invalid instruments and improves the causal estimation and inference. In TWMR analyses, FusioMR$_s$ assesses the causal effect of a risk gene on a single outcome, and FusioMR$_m$ leverages the opportunity that many complex diseases have correlated diseases, subtypes, or comorbidities, which could be affected by shared or correlated risk genes and mechanisms.[27,28] By jointly analyzing these correlated outcomes, FusioMR$_m$ improves the detection of risk genes and offers more comprehensive insights into the underlying causal mechanisms. In addition to TWMR, FusioMR models can also be applied to complex trait exposures.

We performed extensive simulation studies to compare FusioMR to other methods in various scenarios. We demonstrated the flexibility and broad applicability of FusioMR through three different applications. Using FusioMR$_s$, we analyzed single-cell eQTL data from human brains and identified genes associated with Alzheimer disease (AD) in specific cell types, despite the limited sample sizes of these studies. Applying FusioMR$_m$, we jointly analyzed alternative polyadenylation (APA) traits as risk exposures for two correlated outcomes, atrial fibrillation (AF) and ischemic stroke (IS), and identified APA events with effects on either or both diseases. Many of the identified genes with significant APA effects were not detected using other approaches. We also applied FusioMR$_m$ to jointly study the effect of low-density lipoprotein (LDL) on IS risk in the European (EUR) and South Asian (SAS) populations. LDL is a complex trait exposure with a large number of IVs. By borrowing information from the well-powered EUR data, FusioMR$_m$ improved the estimation and inference in SAS.

Methods

FusioMR$_s$: A single-outcome MR model allowing pleiotropy

The FusioMR$_s$ model estimates the causal effect of an exposure trait on a single outcome trait/disease (see Figure 1A). In the context of TWMR analysis, we consider K independent QTLs as IVs. Let γ_k and Γ_k denote the true IV-to-exposure (i.e., QTL) and IV-to-outcome (i.e., GWAS) association effects for the k-th IV ($k = 1,\cdots,K$), respectively. Denote $\{\widehat{\gamma}_k, \widehat{s}_{\gamma k}\}$ as the estimated genetic effect on exposure and its standard error for the k-th variant, obtained from the QTL study. Denote $\{\widehat{\Gamma}_k, \widehat{s}_{\Gamma k}\}$ as the estimated genetic effect on outcome and its standard error for the k-th variant, obtained from the GWAS. We model the effects of the k-th IV as follows:

$$\begin{pmatrix}\widehat{\gamma}_k\\ \widehat{\Gamma}_k\end{pmatrix} \sim \mathcal{N}\left(\begin{pmatrix}\gamma_k\\ \Gamma_k\end{pmatrix}, \widehat{\boldsymbol{S}}_k^{(1)}\boldsymbol{C}^{(1)}\widehat{\boldsymbol{S}}_k^{(1)}\right), \qquad \text{(Equation 1)}$$

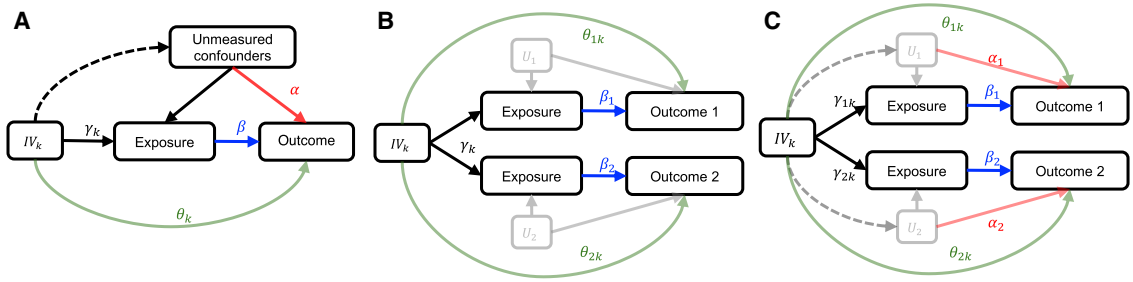

Figure 1. Illustration of the proposed FusioMR models
(A) Single-outcome model accounting for uncorrelated horizontal pleiotropic (UHP) and correlated horizontal pleiotropic (CHP) effects.
(B) Multi-outcome model accounting for UHP effects.
(C) Multi-outcome model accounting for both UHP and CHP effects. Arrows and labels in blue represent the effect mediated by the exposure, green indicates UHP effects, and red indicates CHP effects.

where $\boldsymbol{C}^{(1)}$ is the correlation matrix due to overlapping samples or population substructure, which is often estimated *a priori* and is treated as known.[29] $\widehat{\boldsymbol{S}}_k^{(1)} = \mathrm{diag}(\widehat{s}_{\gamma k}, \widehat{s}_{\Gamma k})$ represents the estimation error from the QTL study and the GWAS. We further assume a linear relationship between the genetic effect on outcome (Γ_k) and the genetic effect on exposure (γ_k):

$$\Gamma_k = \theta_k + \beta \cdot \gamma_k + \alpha \cdot \eta_k \cdot \gamma_k, \qquad \text{(Equation 2)}$$

where β is the causal effect of interest, and θ_k is the UHP effect. We introduce η_k as a latent binary variable with value one indicating that the k-th IV is associated with unmeasured confounders, i.e., with the CHP effect. α represents the strength of the CHP effect and is assumed to scale proportionally with the strength of the IV-to-exposure association effect size (γ_k).[22] As shown in Figure 1A, the total effect of the k-th IV on the outcome, Γ_k, is decomposed into three parts: the effect mediated through exposure ($\beta\gamma_k$, the blue arrow), the UHP effect (θ_k, the green arrow) and the CHP effect ($\alpha\eta_k\gamma_k$, the red arrow). By plugging Equation 2 into Equation 1 and combining models across all IVs, we can write out the full likelihood and build a Bayesian hierarchical model. We assume that $\gamma_k \sim N\left(0, \sigma_\gamma^2\right)$, $\theta_k \sim N(0, \sigma_\theta^2)$, $\eta_k \sim$Bernoulli(π_k), and choose conjugate priors for the latent variables. A Gibbs sampler is used to estimate model parameters (more details are presented in the Note S1).

We perform inference using posterior samples retained after the initial burn-in. The causal effect is estimated using the posterior mean, and the credible interval is defined by the quantiles of the posterior distribution. To quantify the significance of the posterior evidence against the null hypothesis in a way that is comparable to the frequentist p value, we report a Bayesian tail probability, $2 \times \min(\widehat{F}(0), 1 - \widehat{F}(0))$,[30,31] which serve as a pseudo p value. Here $F(x)$ is the empirical cumulative distribution function of the posterior for the causal effect. $F(0)$ is the value of $F(x)$ evaluated at 0 and can be estimated by the proportion of posterior samples less than zero. This pseudo p value is numerically close to the two-sided frequentist p value from a Wald test when the posterior distribution is approximately Gaussian.[30] The pseudo p value can be used for risk gene prioritization and multiple testing adjustment. In addition, the posterior distributions and posterior probabilities can be applied in downstream analysis, such as multi-context risk gene mapping, network reconstruction, and other post-hoc investigations.

When a complex trait is used as exposure and the number of IVs is sufficiently large, FusioMR provides an unbiased estimate for the causal effect by explicitly modeling complex pleiotropy structure. All genetic variants are allowed to have UHP effects, and a subset, $\{k{:}\eta_k = 1\}$, may also have CHP effects. When applying to molecular traits and the number IVs is limited, the CHP effect may not be identifiable, and FusioMR provides the option to adopt a UHP-only model by assigning all $\eta_k = 0$. FusioMR improves estimation by setting empirically derived priors for variance parameters that capture the gene-region-specific characteristics, including the number, strength, and LD structure of its *cis*-QTLs used as IVs. For example, given the IV-to-outcome effects, gene regions with many strong and independent (sparser LD structures) *cis*-QTLs tend to have a larger variance component attributed to exposure than to pleiotropy in Equation 2, resulting in a higher value of σ_γ^2. In contrast, gene regions where IVs have weaker or heterogeneous effects tend to show a larger variance component in the total effect attributed to pleiotropy, leading to a higher value of σ_θ^2. Unlike existing MR methods that impose the same prior across gene regions and implicitly assume homogeneous genetic architectures across the genome,[4,19,24] FusioMR estimates region-specific priors. Specifically, the prior mean for the variance components is estimated as a weighted average of the local de-noised moment estimate and the global empirical mean, with weights depending on the number of IVs (see Note S1 for details). By combining these priors with sampling-based inference, FusioMR enables more accurate variance estimation and more robust causal conclusions, especially when the number of instruments is limited.

FusioMR$_m$: Multi-outcome MR models accounting for shared pleiotropy

Many complex diseases, such as AF and stroke or type 2 diabetes and obesity, share overlapping genetic architectures and biological pathways. This makes joint analysis a powerful strategy for uncovering shared causal mechanisms. In TWMR analysis, jointly analyzing genetically correlated disease outcomes can increase power and facilitate risk gene mapping, especially when the number of instruments is small or when instruments are weak but can be shared across outcomes. We propose FusioMR$_m$ models to simultaneously assess the effects of two correlated exposures on two correlated outcomes by leveraging shared information.

Given the often limited availability of QTLs as IVs, we first focus on the following UHP-only model for TWMR analysis (see Figure 1B for an illustration):

$$\begin{pmatrix} \widehat{\gamma}_{1k} \\ \widehat{\Gamma}_{1k} \\ \widehat{\gamma}_{2k} \\ \widehat{\Gamma}_{2k} \end{pmatrix} \sim \mathcal{N}\left(\begin{pmatrix} \gamma_{1k} \\ \theta_{1k} + \beta_1 \gamma_{1k} \\ \gamma_{2k} \\ \theta_{2k} + \beta_2 \gamma_{2k} \end{pmatrix}, \widehat{\boldsymbol{S}}_k^{(2)} \boldsymbol{C}^{(2)} \widehat{\boldsymbol{S}}_k^{(2)} \right). \quad \text{(Equation 3)}$$

Here β_1 and β_2 represent the causal effects of the two exposures on outcome 1 and outcome 2, respectively. The true IV-to-exposure effects are denoted by γ_{1k} and γ_{2k}, while θ_{1k} and θ_{2k} capture the UHP effects of the k-th instrument on outcome 1 and outcome 2. The matrix $\widehat{\boldsymbol{S}}_k^{(2)} = \mathrm{diag}(\widehat{s}_{\gamma 1k}, \widehat{s}_{\Gamma 1k}, \widehat{s}_{\gamma 2k}, \widehat{s}_{\Gamma 2k})$ represents the standard errors of the estimated effect sizes for QTL studies and GWASs, and $\boldsymbol{C}^{(2)}$ models their correlation structure due to sample overlap. The UHP-only FusioMR$_m$ models the dependence between the two exposures by imposing a bivariate normal prior, $(\gamma_{1k}, \gamma_{2k})^\top \sim N(0, \Sigma_\gamma)$, where Σ_γ is the covariance. Similarly, we model the dependence between UHP effects across outcomes with the prior, $(\theta_{1k}, \theta_{2k})^\top \sim N(0, \Sigma_\theta)$, where Σ_θ is the covariance. The correlated priors on IV-to-exposure and UHP effects enable information sharing across exposures and outcomes while preserving flexibility in causal effect estimation by not directly imposing correlated structure on the causal effect parameters themselves. As a result, FusioMR$_m$ estimates the causal effect for each exposure-outcome pair independently, accounting for shared pleiotropy and without enforcing shared causal effects, thereby ensuring valid and outcome-specific inference. When the exposures share many instruments and exhibit correlation, this joint modeling framework enhances statistical power and estimation precision. It is particularly advantageous when one exposure or outcome has a larger sample size, allowing information sharing to improve inference for the exposure or outcome with more limited data. In contrast, when the two exposures share few or no instruments, FusioMR$_m$ reduces to two independent FusioMR$_s$ models, while still maintaining valid inference.

The framework defined in Equation 3 can be applied to various biological settings. For example, FusioMR$_m$ can be used to examine two molecular trait exposures (e.g., APA and gene expression) in the same *cis*-gene region. Alternatively, it can be applied to analyze the same gene expression in two cell types for two correlated diseases by setting $\gamma_{1k} = \gamma_{2k}$. In this case, FusioMR$_m$ still provides outcome-specific causal effect estimates while leveraging shared instruments and correlation across outcomes.

When the number of IVs is large, we propose the following FusioMR$_m$ model that accounts for both UHP and CHP, as shown in Figure 1C. The model assumes that all IVs may have UHP effects, and a subset has CHP effects:

$$\begin{pmatrix} \widehat{\gamma}_{1k} \\ \widehat{\Gamma}_{1k} \\ \widehat{\gamma}_{2k} \\ \widehat{\Gamma}_{2k} \end{pmatrix} \sim \mathcal{N}\left(\begin{pmatrix} \gamma_{1k} \\ \theta_{1k} + \beta_1 \gamma_{1k} + \alpha_1 \eta_{1k} \gamma_{1k} \\ \gamma_{2k} \\ \theta_{2k} + \beta_2 \gamma_{2k} + \alpha_2 \eta_{2k} \gamma_{2k} \end{pmatrix}, \widehat{\boldsymbol{S}}_k^{(2)} \boldsymbol{C}^{(2)} \widehat{\boldsymbol{S}}_k^{(2)} \right). \quad \text{(Equation 4)}$$

In model (4), FusioMR$_m$ further models the indicators of an IV being associated with confounders for the two outcomes, (η_{1k}, η_{2k}), thereby identifying IVs with and without CHP effects by borrowing information across outcomes. We impose the multinomial prior, $(\eta_{1k}, \eta_{2k})^\top \sim \mathrm{multinomial}(p_{00}, p_{01}, p_{10}, p_{11})$, where each hyper-parameter p_{st}, $s,t \in \{0,1\}$, measures the probability that an IV has CHP effect on outcome 1 (if $s = 1$) and/or outcome 2 (if $t = 1$). The whole profile of $\{p_{..}\}$ depicts the dependence structure among the IVs with and without CHP effects. The rationale is that for genetically correlated outcomes, if an IV is associated with unmeasured confounders for one outcome, particularly the one with a larger sample size, it is more likely to be confounded for the other correlated outcome. By jointly modeling these shared latent indicators, FusioMR$_m$ improves the detection of invalid IVs with CHP effects and reduces bias from invalid instruments. Note that all IVs contribute to the causal effect estimation, while the ones being estimated to be confounded will be downweighted. FusioMR$_m$ improves statistical power for the outcome with limited sample sizes, especially when IVs associated with confounding are shared between the two outcomes, and this is often observed when the two outcomes share underlying genetic mechanisms.[23] When outcomes are uncorrelated and pleiotropy is not shared, FusioMR$_m$ reduces to two independent FusioMR$_s$ models, while still providing valid inference for each. See Note S1 for additional details on the estimation algorithm.

Accounting for sample overlap

To allow overlapping samples between exposure and outcome studies, we can rewrite the distribution for summary statistics in Equation 1 as a joint distribution over all IVs. For FusioMR$_s$ model,

$$\begin{pmatrix} \widehat{\boldsymbol{\gamma}} \\ \widehat{\boldsymbol{\Gamma}} \end{pmatrix} \sim \mathcal{N}\left(\begin{pmatrix} \boldsymbol{\gamma} \\ \boldsymbol{\theta} + \beta \cdot \boldsymbol{\gamma} + \alpha \cdot \boldsymbol{\eta} \circ \boldsymbol{\gamma} \end{pmatrix}, \begin{pmatrix} \widehat{\boldsymbol{S}}_{\boldsymbol{\gamma}} & 0 \\ 0 & \widehat{\boldsymbol{S}}_{\boldsymbol{\Gamma}} \end{pmatrix} (\boldsymbol{C}^{(1)} \otimes \boldsymbol{I}_K) \begin{pmatrix} \widehat{\boldsymbol{S}}_{\boldsymbol{\gamma}} & 0 \\ 0 & \widehat{\boldsymbol{S}}_{\boldsymbol{\Gamma}} \end{pmatrix} \right), \quad \text{(Equation 5)}$$

where $\widehat{\boldsymbol{\gamma}} = (\widehat{\gamma}_1, \cdots, \widehat{\gamma}_K)$ and $\widehat{\boldsymbol{\Gamma}} = (\widehat{\Gamma}_1, \cdots, \widehat{\Gamma}_K)$ are vectors for the marginal effect sizes in exposure and outcome traits, respectively; $\widehat{\boldsymbol{S}}_{\boldsymbol{\gamma}} = \mathrm{diag}(\widehat{s}_{\gamma 1}, \cdots, \widehat{s}_{\gamma K})$ and $\widehat{\boldsymbol{S}}_{\boldsymbol{\Gamma}} = \mathrm{diag}(\widehat{s}_{\Gamma 1}, \cdots, \widehat{s}_{\Gamma K})$ are the corresponding diagonal matrices for standard errors. $\boldsymbol{I}_K$ is a K-dimensional identity matrix. $\circ$ denotes element-by-element product. $\otimes$ denotes Kronecker product. We propose a similar Bayesian hierarchical model to account for overlapping samples that explicitly models the correlation between sampling errors in the Iv-to-exposure and IV-to-outcome effect estimates, as specified by $\boldsymbol{C}^{(1)}$. See Note S1 for additional details for likelihood and posterior distributions. We can extend the FusioMR$_m$ model in Equations 3 and 4 to account for sample overlap in a similar way.

Simulation study

We conducted extensive simulation studies to compare the performance of FusioMR and competing MR methods under a range of scenarios designed for TWMR and complex-trait MR analyses.

We first simulated individual-level genotype and phenotype data, and obtained the marginal summary statistics for SNP-exposure and SNP-outcome associations by fitting linear regressions. We selected the IVs based on the marginal p values for SNP-exposure associations. We retained only the simulation replicates with a sufficient number of IVs. We applied FusioMR and competing MR methods using the same set of IVs within each replicate to ensure fair comparison. We evaluate the estimation biases, root mean squared errors (RMSE), type I error rates, and statistical powers for FusioMR and other frequentist methods. For MR^2, we reported the marginal posterior probability of inclusion (mPPI) and the power calibrated to control the false positive rate under the null.

Existing MR methods were implemented using publicly available R packages with default parameter settings unless otherwise

specified. IVW, MR-Egger, and cML were implemented using the `MendelianRandomization` package.[32] cisMR-cML and MR^2 were implemented using the R packages `cisMRcML`[33] and `MR2`,[34] respectively. For MR^2, the key parameter `EVgamma`, which specifies the prior probability of a non-zero exposure-outcome association, was specified as a single value in (0,1). The default two-parameter vector specification is not appropriate for simulation scenarios with only one or two exposures or outcomes. For cML and cisMR-cML, the data-perturbation (DP) versions were used to improve robustness in *cis*-MR settings. All simulations were conducted in R (version 4.5.1). Scenario-specific data-generating mechanisms, parameter values, and additional implementation details are provided in Note S2.

Data processing and analysis pipeline

We applied FusioMR to three real-data analyses. We first harmonized the effect size summary statistics from the exposure and the outcome datasets to ensure that the effect allele and reference allele were aligned. We then selected SNPs with p values for the effect on exposure below a specified threshold. In analyses 1 and 2, the exposures were molecular traits, and IVs were selected from *cis*-SNPs for each gene. In analysis 3, the exposure was a complex trait, and IVs were selected from genome-wide SNPs. To obtain approximately independent instruments, we performed LD clumping using the `ld_clump` function from the R package `ieugwasr`,[35] with population-matched LD reference panels from the 1000 Genomes Project.[36] The EUR ancestry reference was used for analyses 1 and 2, and the SAS ancestry reference was used for analysis 3.

UHP-only FusioMR models were run independently for each gene-cell-type or gene-tissue pair, and genes with fewer than five IVs were excluded to ensure stable estimation. In analysis 3, FusioMR$_m$ model accounting for both UHP and CHP was used. For the joint analysis integrating EUR and SAS populations, SNPs were first selected using a population-specific p value threshold, and then the intersection was taken. Unless stated otherwise, a Bonferroni-adjusted threshold of 0.05 within each analysis was used to identify significant causal effects. Validation and ancillary analyses using alternative datasets followed the same analysis pipeline. In all three analyses, we assumed no sample overlap between exposure and outcome data.

This unified pipeline was applied across all three analyses, while analysis-specific settings (p value threshold, LD clumping window width and r^2, and population-specific parameters) are described in detail in the results section.

Results

Simulations to evaluate the performance of FusioMR and competing methods

We conducted simulation studies to evaluate the performance of FusioMR models in comparison with existing MR methods in various scenarios.

Simulation 1: MR with a single outcome

In this simulation, we evaluated the performance of FusioMR$_s$ in comparison with existing single-outcome MR methods. We first focused on the TWMR analysis, where the sample size of the exposure study (i.e., an eQTL study) is limited. We simulated individual-level data for GWAS of the outcome (sample size = 20,000) and eQTL study of the exposure (sample size = 300). For each gene, we generated genotype matrices consisting of 200 independent SNPs. All SNPs were assumed to have UHP effects, and a subset (0%, 5%, or 10%) were assumed to have additional CHP effects on the outcome. We sampled IV-to-exposure effects, UHP effects, and CHP effects from Unif(-0.3,0.3), Unif(-0.06,0.06) and Unif(-0.03,0.03), respectively. We generated 2,000 datasets, and retained 600 that had at least 5 IVs after applying the p-value threshold of 0.001 (median number of IVs = 6). Additional simulation details are provided in the Note S2.

We compared FusioMR$_s$ with existing single-outcome MR methods, including IVW-fixed,[4] MR-Egger,[19] and the data-perturbation version of cML[24] (cML-DP). These methods were originally developed for complex traits as exposures, where the number of IVs is typically much larger than in TWMR settings. We also included the data-perturbation version of cisMR-cML[26] (cisMR-cML-DP) as a comparison method, which was designed specifically for *cis*-MR analyses with limited and potentially correlated IVs. For cML-DP and cisMR-cML-DP, we used the default of 200 perturbations. For cisMR-cML-DP, we used conditional rather than marginal effect estimates as inputs.

We evaluated and compared both type I error rate and statistical power. For FusioMR$_s$, we defined type I error rate and power as the proportion of 95% credible intervals that exclude 0 under the null and alternative hypotheses, respectively. For frequentist methods, type I error and power were defined as proportions of replicates with p value below 0.05 for rejecting the null. As shown in Table 1, FusioMR$_s$ controlled type I error rate well and achieved comparatively high power. In contrast, IVW, which does not account for horizontal pleiotropy, showed substantial inflation in type I error rates. Both cML-DP and cisMR-cML-DP also fail to control type I error rates. While MR-Egger showed only mild type I error rate inflation, its power was substantially lower than ours. Moreover, in the context of TWMR analysis, the UHP-only FusioMR$_s$ model remained robust in settings where a subset of IVs had CHP effects. This is because FusioMR$_s$ empirically estimates gene-region-specific priors for pleiotropy. In regions affected by CHP, it tends to assign larger priors to the UHP variance component even without modeling CHP, and that reduces the influence of those IVs and helps control type I error rates.

In Tables S1 and S2, we showed that the inference of FusioMR$_s$ is insensitive to the choice of parameters in the prior for variance. We evaluated average bias and root mean squared error (RMSE) of the estimated causal effect. All methods except MR-Egger achieves small bias and comparable RMSE under the null (Tables S3 and S4). To compare with LD-aware MR methods, we next extended our data generation scheme to allow correlated genetic variants. We included both cisMR-cML-BIC and cisMR-cML-DP methods in comparison. We also included

Table 1. Simulation results comparing FusioMR$_s$ and competing single-outcome MR methods in the settings of a small number of IVs

Type I error rate (nominal level = 0.05)					
IVs with CHP	FusioMR$_s$	IVW	MR-Egger	cML-DP	cisMR-cML
0%	0.052	0.588	0.137	0.125	0.107
5%	0.054	0.597	0.119	0.122	0.118
10%	0.052	0.577	0.121	0.129	0.108
Power (true causal effect = 0.2)					
IVs with CHP	FusioMR$_s$	IVW	MR-Egger	cML-DP	cisMR-cML
0%	0.796	0.990	0.130	0.554	0.415
5%	0.774	0.992	0.120	0.554	0.453
10%	0.775	0.993	0.123	0.570	0.449
Power (true causal effect = 0.3)					
IVs with CHP	FusioMR$_s$	IVW	MR-Egger	cML-DP	cisMR-cML
0%	0.963	0.998	0.128	0.872	0.682
5%	0.962	1.000	0.105	0.851	0.668
10%	0.972	1.000	0.130	0.865	0.686

We varied the proportion of IVs that have CHP effects. We used the UHP-only FusioMR$_s$ model in this simulation.

generalized IVW (gIVW)[37] and generalized MR-Egger (gEgger),[38] which uses generalized linear regression to account for LD among correlated SNPs, as comparison. We assumed an AR(1) auto-regressive correlation structure among genetic variants and used the true underlying correlation matrix as the input. We examined the setting of small QTL sample size ($n_x = 1000$) with all IVs being valid (Table S5) and a subset of IVs with balanced UHP effects (Table S6). We used p value threshold of 1×10^{-5} to select IVs and the median number of IVs is 6–14. When LD is high, FusioMR shows mild inflation, while cisMR-cML-BIC controls type I error rate well by explicitly modeling for the LD structure. When the proportion of IVs with UHP effect is high, cisMR-cML-BIC shows an inflated type I error due to the violation of plurality assumption. cisMR-cML-DP and gEgger tend to be conservative. Even though FusioMR$_s$ does not explicitly models LD, it adapts its variance priors to local LD structure. When LD is moderately high, the empirical variance of $\widehat{\gamma}_j$ inflates because of local clustering. The Empirical-Bayes estimate $\widehat{\sigma}^2_\gamma$ computed from these observed $\widehat{\gamma}^2_j$ (without explicit LD correction) tends to be larger, providing wider variance prior and imposing less shrinkage on the causal estimate. FusioMR's empirical prior adaptively adjusts to different LD correlations.

We next examined a scenario in which the exposure is a complex trait and the number of IVs is moderate to large. In this setting, the GWAS sample sizes for both the exposure and the outcome were set to 20,000. We sampled UHP and CHP effects from Unif(-0.03,0.03) and Unif(-0.05,0.05), respectively. All other simulation settings are the same as the previous scenario. We used a more stringent IV selection threshold of 1×10^{-5}, and the median number of IVs was 140. We repeated the simulation 600 times. As shown in Table 2, FusioMR$_s$ (allowing CHP), MR-Egger, and cML-DP controlled type I error rates well, while IVW showed high inflation. FusioMR$_s$ achieved the highest power, followed by cML-DP.

To investigate the impact of high proportion of IVs with CHP effect, we generated exposure data from a large sample size ($n_x = 20{,}000$) and assumed all IVs have UHP effect and up to 50% of IVs have CHP effect. CHP effects are sampled from Unif (−0.04,0.04). As shown in Table S7, all methods have a higher type I error rate as the proportion of IVs with CHP increases, due to the difficulty in distinguishing the causal effect and CHP effect. cML-DP is conservative but suffers a large power loss When the proportion of IVs with CHP is high (40%–50%). FusioMR$_s$ provides a good balance between robustness and efficiency under increasing CHP, achieving high power with modest inflation.

To evaluate the impact of different distributions of pleiotropic effect, we sampled UHP and CHP effect from normal distributions instead of uniform distributions. To ensure that the pleiotropic contributions to the variance in outcome remained the same, we matched the mean and variance of the normal distributions to those used in the previous uniform setting. Comparing Table 2 (Uniform) and Table S8 (Normal), the inference performance of the different methods is not sensitive to the assumed prior distribution form of pleiotropic effects.

Simulation results also show the robustness of FusioMR to the sparsity of UHP effect (Table S9) and the choice of p value threshold for IV selection (Table S10). The FusioMR model can benefit from modeling the correlation between IV-to-exposure and IV-to-outcome effects when there is a sample overlap (Table S11).

In summary, FusioMR$_s$ consistently demonstrated better control of type I error rates and higher statistical

Table 2. Simulation results comparing FusioMR$_s$ and competing single-outcome MR methods in the settings of a large number of IVs

Type I error rate				
IVs with CHP	FusioMR$_s$	IVW	MR-Egger	cML-DP
0%	0.044	0.315	0.035	0.062
5%	0.054	0.325	0.055	0.068
10%	0.062	0.385	0.067	0.067
Power (true causal effect = 0.02)				
IVs with CHP	FusioMR$_s$	IVW	MR-Egger	cML-DP
0%	0.655	0.924	0.113	0.362
5%	0.668	0.947	0.137	0.373
10%	0.637	0.947	0.163	0.367
Power (true causal effect = 0.025)				
IVs with CHP	FusioMR$_s$	IVW	MR-Egger	cML-DP
0%	0.837	0.980	0.145	0.538
5%	0.865	0.988	0.182	0.553
10%	0.840	0.983	0.210	0.535

We varied the proportion of IVs that have CHP effects. We used the UHP-only FusioMR$_s$ model in this simulation.

power compared to existing single-outcome MR methods, in settings with both limited and large numbers of IVs.

Simulation 2: MR with two outcomes

We first consider a scenario with two correlated outcomes and a molecular trait as the shared exposure (similar to our second data analysis in this work). We generated individual-level GWAS data for two outcomes (sample size = 80,000 and 20,000) and the exposure (sample size = 300). We assumed that IVs have UHP effects but no CHP effects on outcomes. We generated IV-to-exposure effects and UHP effects from Unif(-0.3,0.3) and Unif(-0.1,0.1), respectively. We assumed that the UHP effect sizes are correlated due to the correlation between the two outcome traits. We used a p value threshold of 0.001 to select IVs. We repeated the simulation 2,000 times and evaluate MR methods on 600 of them with at least 5 IVs (the median number of IVs is 6). In addition to the single-outcome MR methods compared in Simulation 1, we also included the multi-response MR method, MR^2,[25] for comparison.

Table 3 showed that both UHP-only FusioMR$_s$ and FusioMR$_m$ control type I error rates. When there is no correlation of pleiotropy between the two outcomes (UHP effect size correlation = 0), FusioMR$_m$ has a similar power as FusioMR$_s$. As the correlation between the UHP effect sizes is getting stronger, FusioMR$_m$ achieves a higher power improvement. FusioMR$_m$ shows a higher power than MR^2, highlighting its advantage in causal effect estimation when the number of IVs is limited (Table S12). Similar to the simulation on a single outcome, other MR methods fail to control type I error rate at the nominal level. All methods in Table S13 showed low biases and comparable RMSE except MR-Egger.

Next, we simulated two correlated complex trait exposures and outcomes. For example, this could be two exposure-outcome trait pairs from two populations (similar to our third data analysis in this work). We aim to examine whether the population with the larger sample size can improve the causal estimation and inference of the smaller population. The GWAS sample sizes for the larger population were set to be $N = 50{,}000$ (for both exposure and outcome), and $N = 5{,}000$ for the smaller population. We sampled UHP and CHP effects from Unif(-0.02,0.02) and Unif(-0.05,0.05), respectively. We assumed a correlation of 0.4 between the UHP effect sizes for the two outcomes. Similarly, the binary indicators of whether an IV has a CHP effect were also assumed to be correlated with a coefficient of 0.4. All other simulation settings are the same as the previous scenario. We selected variants with p value $< 1 \times 10^{-5}$ in either population as IVs in the joint analysis. We repeated the simulation 600 times.

We compared the type I error rate and power for the outcome with the smaller sample size. As shown in Table 4, FusioMR$_m$, FusioMR$_s$, MR-Egger, and cML-DP controlled the type I error rates well, although cML-DP showed deflation and IVW showed mild inflation. The performance of MR^2 improved substantially and became less sensitive to prior when the number of IVs increased (Table S12). Simulation results also showed that FusioMR$_m$ method is robust to different levels of correlation between UHP effect sizes and correlation between CHP indicators (Tables S15, S16, and S17).

Data analysis 1: Mapping cell-type-specific risk genes for AD via FusioMR$_s$

We applied FusioMR$_s$ to map risk genes for AD, leveraging single-cell eQTL (sc-eQTL) statistics and GWAS summary

Table 3. Simulation results comparing FusioMR$_m$, FusioMR$_s$, and competing MR methods in the settings of two outcomes with a shared molecular trait exposure

Type I error rate						
UHP correlation	FusioMR$_m$	FusioMR$_s$	IVW	MR-Egger	cML-DP	cisMR-cML
0	0.056	0.041	0.730	0.134	0.175	0.165
0.4	0.066	0.053	0.732	0.139	0.171	0.146
0.8	0.071	0.048	0.694	0.124	0.169	0.156
Power (true causal effect = 0.3)						
UHP correlation	FusioMR$_m$	FusioMR$_s$	IVW	MR-Egger	cML-DP	cisMR-cML
0	0.725	0.719	0.995	0.131	0.464	0.442
0.4	0.772	0.720	0.987	0.127	0.482	0.459
0.8	0.793	0.735	0.988	0.126	0.482	0.466
Power (true causal effect = 0.4)						
UHP correlation	FusioMR$_m$	FusioMR$_s$	IVW	MR-Egger	cML-DP	cisMR-cML
0	0.922	0.904	1.000	0.127	0.710	0.615
0.4	0.922	0.901	1.000	0.116	0.724	0.617
0.8	0.945	0.906	1.000	0.119	0.714	0.615

FusioMR$_m$ was applied to jointly estimate the causal effects for two outcomes but the comparisons were based on only outcome 1 (the outcome with the smaller sample size). We varied the correlation of UHP effect sizes between the two outcomes.

statistics for the clinical diagnosis of AD. The sc-eQTL summary statistics were obtained from Bryois et al..[39] The study included data of 144–192 individuals from eight brain cell types derived from the prefrontal cortex, temporal cortex and white matter. The eight cell types were astrocytes, excitatory neurons, inhibitory neurons, oligodendrocytes, microglia, oligodendrocyte precursor cells (OPCs), endothelial cells, and pericytes. GWAS summary statistics for AD were obtained from the Religious Orders Study and Memory and Aging Project (ROSMAP), which included 802 cases and 1,629 controls.[40]

We examined 6,681 to 14,028 genes across the eight brain cell types. We selected IVs using a p value threshold of 0.001 and performed the LD clumping at the r^2 threshold of 0.1 in a window of 50kb. After IV selection, the median number of IVs is 3 and there are more than 80% of genes with fewer than 5 IVs. We restricted our analysis to genes with at least 5 IVs and analyzed 240 to 2,202 genes in the eight brain cell types (Table S18).

We applied the UHP-only FusioMR$_s$ together with other single-outcome MR methods, including IVW, MR-Egger, cML-DP, and cisMR-cML-DP to identify risk genes for AD in each cell type. FusioMR$_s$, cisMR-cML-DP, and MR-Egger achieve better inflation control compared with methods not designed for TWMR analysis, such as IVW and cML-DP. MR-Egger is conservative and showed mild deflation (Table S19). At a Bonferroni-adjusted p value threshold of 0.05, FusioMR$_s$ identified 31 genes with significant effects on AD risk in at least one cell type (Tables S18, S19, and S25).

The heatmap in Figure 2 shows the $-log_{10}(p)$ of the significant genes identified by FusioMR$_s$ in the eight cell types. Many of the identified risk genes have been previously reported in the literature as being associated with AD, related diseases, or relevant biological pathways. Our analyses examined their effects on AD risks at the single-cell resolution. We further performed a Gene set enrichment analysis for the set of 31 genes,[41] and found that protein dephosphorylation (GO:0006470) is one of the top biological processes enriched with our identified genes. Tau protein hyperphosphorylation is a hallmark of AD, leading to neurofibrillary tangles.[42] Protein phosphatases, including our identified *PTPN13* (MIM: 600267) (significant in oligodendrocytes, p-value = 2×10^{-5}) and *PPM1E* (MIM: 619308) (inhibitory neurons, p-value = 5×10^{-7}), play a crucial role in tau dephosphorylation and are often dysregulated in AD. We identified *KANSL1* (MIM: 612452) (endothelial cells, p value = 3×10^{-5}; excitatory neurons, p value = 7×10^{-6}; inhibitory neurons, p value = 1×10^{-5}; oligodendrocytes, p value = 3×10^{-6}; OPCs, p value = 2×10^{-5}; pericytes, p value = 1×10^{-4}; astrocytes, p value = 2×10^{-5}), *ARL17B* (endothelial cells, p value = 3×10^{-6}; inhibitory neurons, p value = 3×10^{-7}; excitatory neurons, p value = 3×10^{-7}; oligodendrocytes, p value = 2×10^{-7}; OPCs, p value = 4×10^{-7}; microglia, p value = 7×10^{-7}; astrocytes, p value = 4×10^{-6}), and *MAPT* (MIM: 157140) (astrocytes, p value = 1×10^{-6}) located in the chromosome 17q21.31 region. This region is characterized by a 970 kb inversion polymorphism, defining a haplotype, which has been associated with an increased risk of several neurodegenerative diseases, including AD.[43,44] Additionally, *CR1* (MIM: 120620) (oligodendrocytes, p value = 4×10^{-5}) is a membrane-bound receptor and it plays a role in clearing immune complexes and modulating neuroinflammation, both of which are crucial

Table 4. Simulation results comparing FusioMR$_m$, FusioMR$_s$, and competing MR methods in the settings of two complex trait exposures and outcomes

Type I error rate					
IVs with CHP	FusioMR$_m$	FusioMR$_s$	IVW	MR-Egger	cML-DP
0	0.057	0.068	0.105	0.062	0.033
5%	0.058	0.062	0.100	0.052	0.027
10%	0.055	0.067	0.123	0.072	0.018
Power (true causal effect = 0.025)					
IVs with CHP	FusioMR$_m$	FusioMR$_s$	IVW	MR-Egger	cML-DP
0	0.660	0.613	0.698	0.070	0.453
5%	0.688	0.657	0.747	0.092	0.435
10%	0.692	0.632	0.772	0.097	0.440
Power (true causal effect = 0.03)					
IVs with CHP	FusioMR$_m$	FusioMR$_s$	IVW	MR-Egger	cML-DP
0	0.820	0.753	0.838	0.077	0.575
5%	0.825	0.770	0.847	0.095	0.605
10%	0.827	0.765	0.870	0.105	0.615

FusioMR$_m$ was applied to jointly estimate the causal effects for two outcomes but the comparisons were based on only outcome 1 (the outcome with the smaller sample size). we varied the proportion of IVs that have CHP effects.

in AD.[45] *GDPD1* (MIM: 616317) was identified in astrocytes with a p value of 7×10^{-7}. A previous study investigating blood gene expression markers identified it as with altered expression in early-stage AD patients.[46] GDPD1, as an enzyme involved in lipid metabolism, could influence AD pathology by affecting synaptic function, neuronal communication, and the inflammatory milieu by altering lipid-derived signaling molecules.

To validate our findings, we used a validation sc-eQTL dataset that was generated from dorsolateral prefrontal cortex (DLPFC) samples of 424 individuals of advanced age.[47] This dataset includes all brain cell types in the discovery dataset except pericytes. We used the same IV selection criteria and applied FusioMR$_s$ for each cell type. We found that, out of the 31 identified risk genes from the discovery data, 26 are available in the validation dataset. Among the 26 genes, 23 (88%) were replicated at the p value threshold of 0.05 (Table S18). It should be noted that although the validation sc-eQTL dataset includes samples from the discovery set, it also contains more than half new individuals, providing substantial additional information for validation.

To evaluate whether the cell-type-specific effects identified by FusioMR are detectable in bulk tissue, we performed a parallel TWMR analysis using eQTL data from 13 bulk brain tissues in the GTEx Project.[48] Among the 31 risk genes identified in the sc-eQTL discovery analysis, only 10 were also detected in at least one bulk brain tissue (Tables S20 and S25), primarily in cortical tissues (cortex, anterior cingulate cortex BA24, frontal cortex BA9) and subcortical/cerebellar tissues (caudate basal ganglia, cerebellar hemisphere, cerebellum), corresponding to major cell types in the sc-eQTL data (Figure 2). The remaining 21 genes were uniquely identified in the single-cell analysis, suggesting cell-type-specific effects not captured by bulk data (Table S20). These 21 uniquely identified genes were highly enriched in relatively rare cell types, including endothelial cells (2 out of 3 genes), OPCs (4 out of 5 genes), and pericytes (2 out of 3 genes). For example, *ATP7B* (MIM: 606882) was identified specifically in pericytes (p value $= 2 \times 10^{-5}$), and its dysregulation has been linked to blood-brain barrier dysfunction and pericyte-related neurodegeneration.[49–51]

Data analysis 2: Identifying risk genes for atrial fibrillation and ischemic stroke by integrating APA-QTLs and GWASs via FusioMR$_m$

Alternative polyadenylation is a widespread post-transcriptional regulatory mechanism affecting approximately 70% of human genes. APA modulates transcript stability, localization, and translation by altering 3′ untranslated region (3′UTR) lengths through differential polyadenylation site usage. APA-QTLs have been shown to contribute to complex trait heritability and offer regulatory insights beyond traditional eQTLs.[52–54] Given its regulatory importance, APA is increasingly recognized as a potential mediator of genetic risk for many complex diseases.[55] Yet the role of APA in AF is not well established. AF is a heritable and heterogeneous cardiac arrhythmia, and APA may influence its development by modulating isoform usage of genes involved in ion channel activity, signal transduction, and stress response, which are all key pathways implicated in AF pathogenesis.[56,57] AF is also a major risk factor and therapeutic target for IS, particularly the cardioembolic subtype.[58–61] Prior studies have

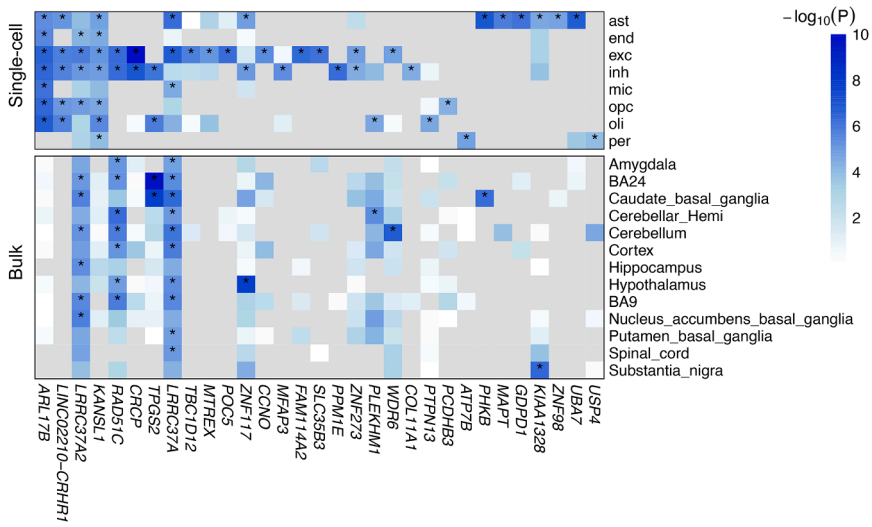

Figure 2. Heatmap comparing AD-associated genes identified using single-cell and bulk eQTL data

Genes significant in at least one cell type in the single-cell analysis were selected. Colors represent $-log_{10}(p)$ from the FusioMR$_s$ analysis for AD diagnosis. Stars indicate genes that pass the Bonferroni-adjusted significance threshold of 0.05. Abbreviations: AD, Alzheimer disease; oli, oligodendrocytes; exc, excitatory neurons; inh, inhibitory neurons; ast, astrocytes; mic, microglia; end, endothelial cells; per, pericytes.

revealed shared genetic loci and biological pathways linking AF and stroke.[62–66]

In this analysis, we applied FusioMR$_m$ to integrate APA-QTL with GWAS summary statistics from AF and IS for detecting APA-mediated risk genes. We used summary statistics for genetic effects on APA from 3′aQTL-atlas, in which APA-QTL were generated from GTEx v8 RNA-seq profiles across multiple tissues from 838 individuals.[53] APA events were quantified as the relative usage of distal polyadenylation sites for each gene.[67] Eighteen biologically relevant tissues were analyzed, including 13 brain tissues, 2 artery tissues, 2 heart tissues, and whole blood. We used GWAS summary statistics for IS from the GIGASTROKE Consortium,[68] comprising 62,100 cases and 1,234,808 controls of European ancestry. AF GWAS data were from Nielsen et al.,[69] including 60,620 cases and 970,216 controls of European ancestry.

We applied the UHP-only FusioMR$_m$ together with single-outcome MR methods, including FusioMR$_s$, IVW, MR-Egger, cML-DP, and cisMR-cML-DP, as well as the multi-outcome method MR^2 to estimate the causal effect of APA events in each of the 18 tissues on AF and IS. A total of 6,638 to 9,591 genes with APA events were analyzed for the 18 tissues (Table S21). We selected the IVs using a p value threshold of 0.001 and performed LD clumping at the r^2 threshold of 0.01 in a window of 50 kb. We restricted our analysis to genes with at least 5 shared IVs, and 183 to 791 genes were tested in the 18 tissues (Table S21). We detected the risk genes at a Bonferroni-adjusted p value threshold of 0.05 in each tissue (Tables S21, S22, and S26). Among comparison methods, FusioMR$_m$, FusioMR$_s$, cisMR-cML-DP, and MR-Egger demonstrated comparatively reasonable genomic inflation control. By borrowing strength across AF and IS, FusioMR$_m$ detected more risk genes than its single-outcome counterpart FusioMR$_s$.

We identified 61 risk genes for AF in at least one tissue via FusioMR$_m$ by jointly analyzing AF and IS, while using FusioMR$_s$ on AF identified 50 risk genes. Among the 61 risk genes, 23 (38%) were detected in two or more tissues, with the highest numbers of significant genes detected in artery aorta (16 APA genes, tissue sample size $N = 439$) and heart atrial appendage (16 APA genes, tissue sample size $N = 444$) (See Tables S23 and S26). Most of the identified genes showed consistent effects across multiple tissues (see Figure S1). Figure 3 shows a heatmap of $-log_{10}(p)$ values for the significant APAs identified by FusioMR$_m$ for both AF and IS in relevant tissues, highlighting distinct yet partially overlapping tissue-specific APA signatures for the two diseases.

Several APA genes identified by FusioMR$_m$ are supported in the literature. *NCF1* (MIM: 608512) and *SHC1* (MIM: 600560) are well-established alternative polyadenylation in humans, as documented across multiple large-scale 3′UTR/cleavage-site resources.[70–72] Extensive animal-model evidence shows APA-mediated modulation of their gene expression implicates a biologically mechanism contributing to AF susceptibility. *NCF1*, encoding the NOX2 activator p47phox, is a critical determinant of reactive oxygen species (ROS) production in the heart. NOX2 activation drives atrial fibrosis, and its genetic deletion or pharmacologic inhibition reduces AF inducibility in mice.[73,74] Similarly, particularly the p66Shc isoform of *SHC1* is a master regulator of mitochondrial ROS and apoptosis, and mice lacking p66Shc are protected from pressure-overload–induced oxidative damage, fibrosis, and maladaptive cardiac remodeling.[75,76] Our APA-based TWMR analysis in human tissues identified significant 3′UTR length changes in both *NCF1* and *SHC1* associated with AF risk. Specifically, we observed that 3′UTR lengthening in *NCF1* (p value $= 5 \times 10^{-6}$ in the whole blood) and 3′UTR shortening in *SHC1* (p value $= 3 \times 10^{-6}$ in the heart left ventricle tissue) is highly associated with increased AF risk.

We further performed FusioMR$_m$ analysis using gene expression levels (rather than APA events) as the exposures. Among the 61 genes with significant APA effects on AF, 53 genes also show significant effects at the gene expression level in at least one tissue. There are 8 (13%) genes uniquely identified in the APA-based TWMR analysis. *PLCL1* (MIM: 600597) (phospholipase C-like 1)

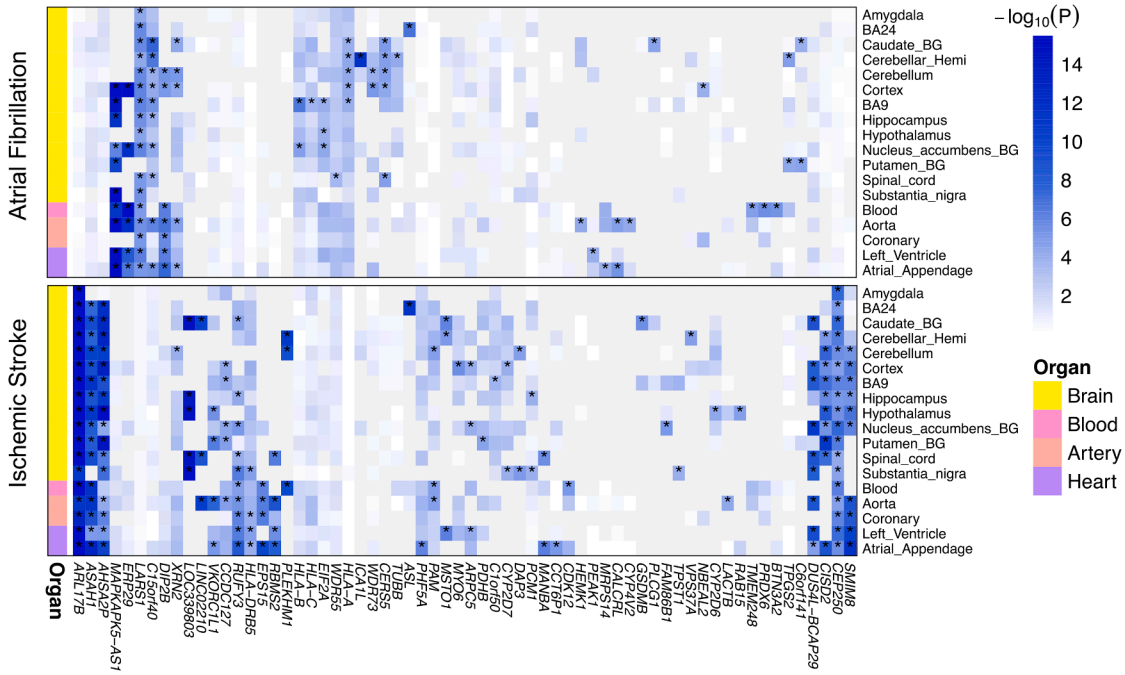

Figure 3. Heatmap of APA genes associated with atrial fibrillation and ischemic stroke across tissues
Genes significant in at least one tissue for either atrial fibrillation or ischemic stroke were selected. Colors represent $-log_{10}(p)$ values from the FusioMR$_m$ analysis across 18 tissues. The upper panel shows associations with atrial fibrillation, and the lower panel shows associations with ischemic stroke. Stars indicate genes that pass the Bonferroni-adjusted significance threshold of 0.05. Abbreviations: APA, alternative polyadenylation.

showed a significant association with AF in coronary artery tissue (p value $= 3 \times 10^{-4}$) in the APA-based TWMR analysis but was not significant in the expression-based TWMR analysis (p value $= 0.39$). A previous GWAS identified the SNP, rs6716898, a variant near *PLCL1*, as a susceptibility locus for AF.[77] *PLCL1* is involved in phosphoinositide signaling, which regulates cardiac electrophysiology, a key process in the pathogenesis of AF.[78,79] Genes uniquely identified through the APA-based TWMR analysis suggest regulatory mechanisms mediated by alternative polyadenylation rather than gene expression levels. These genes may be missed by bulk-tissue expression-based TWMR due to the averaging of isoform usage across cell types and limited resolution of 3′UTR dynamics. Our findings highlight the contribution of APA-based TWMR analysis in revealing regulatory mechanisms and risk associations that are not captured by expression-based analyses.

Data analysis 3: Estimating population-specific causal effect of low-density lipoprotein on ischemic stroke via FusioMR$_m$

LDL cholesterol levels are critical in assessing cardiovascular risk and play distinct roles in the pathophysiology of stroke and its subtypes.[80] A positive association between LDL levels and IS risk has been established in EUR populations.[81–84] However, few studies have assessed this causal relationship in the SAS population, and recent findings have reported a non-significant effect of LDL on IS in individuals of South Asian ancestry.[85] The insignificant result may be due to the limited sample size in SAS or to differences in stroke subtype distribution and the prevalence of key risk factors for IS between EUR and SAS populations.[86,87]

We applied FusioMR$_m$ and MR^2 to estimate the population-specific causal effect of LDL on IS by jointly analyzing data from EUR and SAS, respectively. The IV-to-exposure summary statistics for LDL were obtained from the Global Lipids Genetics Consortium with sample size $N = 1{,}320{,}016$ for EUR ancestry and $N = 146{,}492$ for SAS ancestry.[88] Summary statistics for IS were obtained from the GIGASTROKE consortium,[68] where EUR ancestry consists of 62,100 cases and 1,234,808 controls, and SAS ancestry consists of 3,462 cases and 7,672 controls. SNPs significantly associated with exposures from both populations (p value $\leq 1 \times 10^{-3}$ for SAS and p value $\leq 1 \times 10^{-4}$ for EUR) were selected as IVs, followed by LD clumping with a window of 100 kb and a r^2 threshold of 0.01. We selected 131 IVs. We identified a significant positive causal effect of LDL on IS in the SAS population using FusioMR$_m$ (estimated effect size $= 0.30$, p value $= 0.010$, Figure 4A). MR ^{2} estimated a positive causal effect ($\widehat{\beta} = 0.15$) with moderate support (mPPI $= 0.39$; see Table S24), consistent in direction with the estimate of FusioMR$_m$.

As a comparison, we applied single-outcome MR methods including FusioMR$_s$, IVW, MR-Egger, and cML-DP on only the GWAS of SAS ancestry. We select IVs using p value threshold of 1×10^{-4}, clumping window of 100 kb

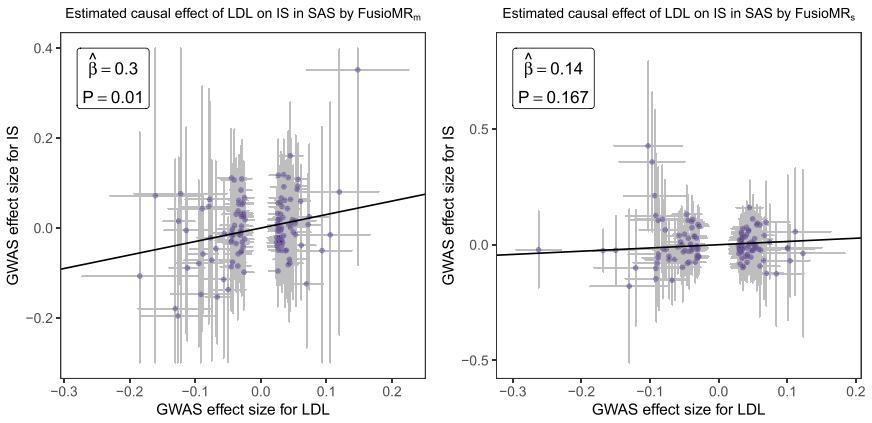

Figure 4. Causal effect estimates of LDL on IS in the SAS population

The horizontal axis represents the IV-LDL effects, and the vertical axis represents the IV-IS effects.

(A) A total of 131 SNPs significantly associated with LDL in both EUR and SAS populations were selected as IVs, and the causal effect of LDL on IS was estimated using FusioMR$_m$.

(B) A total of 133 SNPs significantly associated with LDL in SAS were selected as IVs and, the causal effect of LDL on IS was estimated using FusioMR$_s$. Error bars represent 1.96 times the standard errors of the estimates. Abbreviations: LDL, low-density lipoprotein; IS, ischemic stroke; IV, instrumental variables; EUR, European; SAS, South Asian.

and r^2 threshold of 0.01. We selected 133 IVs. All these single-outcome MR methods produced insignificant causal estimates, although the effect directions were consistently positive (Table S24). Using FusioMR$_s$, the estimated effect size was = 0.14 with a p value of 0.167 (Figure 4B). FusioMR$_m$ enhances the causal effect estimation and causal inference in the SAS population by using shared and consistent IVs and borrowing information from the EUR populations.

Discussion

In this study, we introduced FusioMR, a set of MR models for estimating the causal effects of molecular or complex trait exposures on one or more outcomes. MR has been increasingly applied in recent literature to identify causal genes and molecular risk factors for complex diseases, yet there remains a notable lack of methods specifically addressing the unique challenges in transcriptome-wide MR analyses. FusioMR was motivated by and tailored for TWMR settings, where the number of *cis*-QTLs as IVs is often limited, reducing power and compromising both causal effect identification and inference robustness. For different gene regions, differences in the number of *cis*-QTLs, their LD structures, effect sizes, and effect consistency can significantly influence MR performance. Existing methods have largely overlooked the opportunity to improve TWMR estimation by accounting for gene-region-specific characteristics, particularly when IVs are limited, weak, or correlated. FusioMR fills this gap by estimating empirically derived gene-region-specific priors and employing a sampling-based inference framework. It outputs posterior distributions, posterior probabilities, and frequentist-like pseudo p values to support flexible and interpretable downstream analyses. FusioMR$_s$ estimates the causal effect of an exposure on a single outcome, while FusioMR$_m$ expands the framework to two correlated outcomes. FusioMR$_m$ is motivated by the fact that many complex diseases have correlated diseases, subtypes, or comorbidities, which could be affected by shared or correlated exposures. Jointly analyzing two correlated outcomes allows the study of shared genetic architecture and pleiotropy, improving power and uncovering risk genes that may be missed in single-outcome analyses. Simulation studies demonstrate that both FusioMR$_s$ and FusioMR$_m$ control the type I error rates and achieve high powers, especially in scenarios with limited or weak IVs. FusioMR can also be applied to study complex trait exposures beyond TWMR, accounting for both UHP and CHP. Overall, FusioMR provides a unified modeling framework for both molecular and complex-trait exposures, along with single- and multi-outcome settings that facilitate principled IV selection and evaluation, and support cross-trait inference across diverse MR applications.

We applied FusioMR to three data analyses. Using FusioMR$_s$, we identified cell-type-specific gene expression traits associated with AD, highlighting its effectiveness in detecting risk genes from single-cell data, particularly in rare cell types. We also applied FusioMR$_m$ to detect alternative polyadenylation affecting AF and/or IS. We identified APA-unique risk genes that were otherwise not identified using only single-outcome data and conventional expression-based TWMR analysis. Lastly, we applied FusioMR$_m$ to GWAS summary statistics from European and South Asian populations. FusioMR$_m$ demonstrated improved power for detecting causal effects in the underpowered South Asian cohort by borrowing information from the better-powered European cohort. These applications illustrate the power and flexibility of FusioMR models in identifying molecular traits and complex traits as risk factors for complex diseases.

While FusioMR provides a flexible framework for causal inference with one or two outcomes, the current models have limitations that offer potential opportunities for future development. FusioMR$_s$ is currently limited to analyzing a single exposure, and FusioMR$_m$ focuses on a pair of correlated exposures for two correlated outcomes. Extending the framework to jointly consider multiple exposures for each outcome would provide a more

comprehensive understanding of the relationships among risk factors. Another limitation is that FusioMR$_m$ is restricted to two outcomes. In settings involving more than two correlated outcomes, users could use pairwise analyses, which may not fully capture the correlation structure or shared pleiotropic effects. Expanding FusioMR to accommodate multivariate outcomes and high-dimensional exposure sets represents a potential direction for future methodological innovation. These extensions are non-trivial and would require the development and evaluation of new modeling assumptions. These efforts lie beyond the scope of this work. Last but not least, a major challenge in TWMR analysis is that, with only a small number of *cis*-QTLs available for most genes, it is difficult to reliably distinguish causal effects, UHP, and CHP components. Existing methods rely on different assumptions, and when these assumptions are violated, complementary approaches are needed. Thus, there remains a strong need for additional methods that address these challenges in TWMR analyses.

Data and code availability

This study used the QTL study and GWAS summary datasets that are all publicly available as indicated in their corresponding references. R code for simulation studies and real data analysis is available at https://github.com/kangbw702/FusioMR-analysis. The proposed methods are implemented in R package FusioMR, which is publicly available to download on GitHub at https://github.com/kangbw702/FusioMR.

Acknowledgments

We thank the GTEx Consortium. The research of L.S.C., B.K., and J.C. was supported by NIH 1R01GM154421 and 1U01MH139345.

Author contributions

L.S.C. conceived the project. L.S.C. and B.K. developed the methods and wrote the manuscript. K.X. assisted B.K. with the development of the estimation algorithm. B.K. conducted the simulations and analyzed the data. D.L. assisted with the simulations. S.F. assisted with the software development. All authors provided valuable suggestions for the development of the methods and the data analyses. All authors reviewed and approved the final manuscript.

Declaration of interests

The authors declare no competing interests.

Supplemental information

Supplemental information can be found online at https://doi.org/10.1016/j.ajhg.2026.03.017.

Received: July 25, 2025
Accepted: March 24, 2026
Published: April 16, 2026

References

1. Smith, G.D., and Ebrahim, S. (2003). 'Mendelian randomization': can genetic epidemiology contribute to understanding environmental determinants of disease? Int. J. Epidemiol. *32*, 1–22. https://doi.org/10.1093/ije/dyg070.
2. Didelez, V., and Sheehan, N. (2007). Mendelian randomization as an instrumental variable approach to causal inference. Stat. Methods Med. Res. *16*, 309–330. https://doi.org/10.1177/0962280206077743.
3. Lawlor, D.A., Harbord, R.M., Sterne, J.A.C., Timpson, N., and Davey Smith, G. (2008). Mendelian randomization: using genes as instruments for making causal inferences in epidemiology. Stat. Med. *27*, 1133–1163. https://doi.org/10.1002/sim.3034.
4. Burgess, S., Butterworth, A., and Thompson, S.G. (2013). Mendelian randomization analysis with multiple genetic variants using summarized data. Genet. Epidemiol. *37*, 658–665. https://doi.org/10.1002/gepi.21758.
5. Burgess, S., Small, D.S., and Thompson, S.G. (2017). A review of instrumental variable estimators for Mendelian randomization. Stat. Methods Med. Res. *26*, 2333–2355. https://doi.org/10.1177/0962280215597579.
6. Angrist, J.D., Imbens, G.W., and Rubin, D.B. (1996). Identification of causal effects using instrumental variables. J. Am. Stat. Assoc. *91*, 444–455. https://doi.org/10.1080/01621459.1996.10476902.
7. Angrist, J.D., and Imbens, G.W. (1995). Two-stage least squares estimation of average causal effects in models with variable treatment intensity. J. Am. Stat. Assoc. *90*, 431–442. https://doi.org/10.1080/01621459.1995.10476535.
8. Baiocchi, M., Cheng, J., and Small, D.S. (2014). Instrumental variable methods for causal inference. Stat. Med. *33*, 2297–2340. https://doi.org/10.1002/sim.6128.
9. Gleason, K.J., Yang, F., and Chen, L.S. (2021). A robust two-sample transcriptome-wide Mendelian randomization method integrating GWAS with multi-tissue eQTL summary statistics. Genet. Epidemiol. *45*, 353–371. https://doi.org/10.1002/gepi.22380.
10. Richardson, T.G., Hemani, G., Gaunt, T.R., Relton, C.L., and Davey Smith, G. (2020). A transcriptome-wide Mendelian randomization study to uncover tissue-dependent regulatory mechanisms across the human phenome. Nat. Commun. *11*, 185. https://doi.org/10.1038/s41467-019-13921-9.
11. Wingo, A.P., Liu, Y., Gerasimov, E.S., Gockley, J., Logsdon, B.A., Duong, D.M., Dammer, E.B., Robins, C., Beach, T.G., Reiman, E.M., et al. (2021). Integrating human brain proteomes with genome-wide association data implicates new proteins in Alzheimer's disease pathogenesis. Nat. Genet. *53*, 143–146. https://doi.org/10.1038/s41588-020-00773-z.
12. Zheng, J., Haberland, V., Baird, D., Walker, V., Haycock, P.C., Hurle, M.R., Gutteridge, A., Erola, P., Liu, Y., Luo, S., et al. (2020). Phenome-wide Mendelian randomization mapping the influence of the plasma proteome on complex diseases. Nat. Genet. *52*, 1122–1131. https://doi.org/10.1038/s41588-020-0682-6.
13. Chan, L.S., Malakhov, M.M., and Pan, W. (2024). A novel multivariable Mendelian randomization framework to disentangle highly correlated exposures with application to metabolomics. Am. J. Hum. Genet. *111*, 1834–1847. https://doi.org/10.1016/j.ajhg.2024.07.007.
14. Nakanishi, T., Willett, J., Farjoun, Y., Allen, R.J., Guillen-Guio, B., Adra, D., Zhou, S., and Richards, J.B. (2023).

Alternative splicing in lung influences COVID-19 severity and respiratory diseases. Nat. Commun. *14*, 6198. https://doi.org/10.1038/s41467-023-41912-4.
15. Lu, Y., Xu, K., Maydanchik, N., Kang, B., Pierce, B.L., Yang, F., and Chen, L.S. (2024). An integrative multi-context Mendelian randomization method for identifying risk genes across human tissues. Am. J. Hum. Genet. *111*, 1736–1749. https://doi.org/10.1016/j.ajhg.2024.06.012.
16. Larsson, S.C., and Burgess, S. (2021). Causal role of high body mass index in multiple chronic diseases: a systematic review and meta-analysis of Mendelian randomization studies. BMC Med. *19*, 320. https://doi.org/10.1186/s12916-021-02188-x.
17. Larsson, S.C., Bäck, M., Rees, J.M.B., Mason, A.M., and Burgess, S. (2020). Body mass index and body composition in relation to 14 cardiovascular conditions in UK Biobank: a Mendelian randomization study. Eur. Heart J. *41*, 221–226. https://doi.org/10.1093/eurheartj/ehz388.
18. Oliva, M., Demanelis, K., Lu, Y., Chernoff, M., Jasmine, F., Ahsan, H., Kibriya, M.G., Chen, L.S., and Pierce, B.L. (2023). DNA methylation QTL mapping across diverse human tissues provides molecular links between genetic variation and complex traits. Nat. Genet. *55*, 112–122. https://doi.org/10.1038/s41588-022-01248-z.
19. Bowden, J., Davey Smith, G., and Burgess, S. (2015). Mendelian randomization with invalid instruments: effect estimation and bias detection through Egger regression. Int. J. Epidemiol. *44*, 512–525. https://doi.org/10.1093/ije/dyv080.
20. Qi, G., and Chatterjee, N. (2019). Mendelian randomization analysis using mixture models for robust and efficient estimation of causal effects. Nat. Commun. *10*, 1941. https://doi.org/10.1038/s41467-019-09432-2.
21. Burgess, S., Foley, C.N., Allara, E., Staley, J.R., and Howson, J.M.M. (2020). A robust and efficient method for Mendelian randomization with hundreds of genetic variants. Nat. Commun. *11*, 376. https://doi.org/10.1038/s41467-019-14156-4.
22. Morrison, J., Knoblauch, N., Marcus, J.H., Stephens, M., and He, X. (2020). Mendelian randomization accounting for correlated and uncorrelated pleiotropic effects using genome-wide summary statistics. Nat. Genet. *52*, 740–747. https://doi.org/10.1038/s41588-020-0631-4.
23. Cheng, Q., Zhang, X., Chen, L.S., and Liu, J. (2022). Mendelian randomization accounting for complex correlated horizontal pleiotropy while elucidating shared genetic etiology. Nat. Commun. *13*, 6490. https://doi.org/10.1038/s41467-022-34164-1.
24. Xue, H., Shen, X., and Pan, W. (2021). Constrained maximum likelihood-based Mendelian randomization robust to both correlated and uncorrelated pleiotropic effects. Am. J. Hum. Genet. *108*, 1251–1269. https://doi.org/10.1016/j.ajhg.2021.05.014.
25. Zuber, V., Lewin, A., Levin, M.G., Haglund, A., Ben-Aicha, S., Emanueli, C., Damrauer, S., Burgess, S., Gill, D., and Bottolo, L. (2023). Multi-response Mendelian randomization: Identification of shared and distinct exposures for multimorbidity and multiple related disease outcomes. Am. J. Hum. Genet. *110*, 1177–1199. https://doi.org/10.1016/j.ajhg.2023.06.005.
26. Lin, Z., and Pan, W. (2024). A robust cis-Mendelian randomization method with application to drug target discovery. Nat. Commun. *15*, 6072. https://doi.org/10.1038/s41467-024-50385-y.
27. Parkes, M., Cortes, A., Van Heel, D.A., and Brown, M.A. (2013). Genetic insights into common pathways and complex relationships among immune-mediated diseases. Nat. Rev. Genet. *14*, 661–673. https://doi.org/10.1038/nrg3502.
28. Sivakumaran, S., Agakov, F., Theodoratou, E., Prendergast, J.G., Zgaga, L., Manolio, T., Rudan, I., McKeigue, P., Wilson, J.F., and Campbell, H. (2011). Abundant pleiotropy in human complex diseases and traits. Am. J. Hum. Genet. *89*, 607–618. https://doi.org/10.1016/j.ajhg.2011.10.004.
29. Urbut, S.M., Wang, G., Carbonetto, P., and Stephens, M. (2019). Flexible statistical methods for estimating and testing effects in genomic studies with multiple conditions. Nat. Genet. *51*, 187–195. https://doi.org/10.1038/s41588-018-0268-8.
30. Gelman, A., Carlin, J.B., Stern, H.S., Dunson, D.B., Vehtari, A., and Rubin, D.B. (2013). Bayesian Data Analysis, 3 edition (Chapman and Hall/CRC). https://doi.org/10.1201/b16018.
31. Gelman, A., Meng, X.-L., and Stern, H. (1996). Posterior predictive assessment of model fitness via realized discrepancies. Statistica *6*, 733–760. http://www.jstor.org/stable/24306036.
32. Burgess, S. & Yavorska, O. MendelianRandomization: Mendelian Randomization Package. R package version 0.10.0, https://CRAN.R-project.org/package=MendelianRandomization (2024).
33. Lin, Z. cisMRcML: A robust cisMR method based on constrained maximum likelihood. R package version 0.0.0.9000. https://github.com/ZhaotongL/cisMRcML (2025).
34. Bottolo, L. & Zuber, V. MR2: Bayesian multi-response Mendelian randomisation. R package version 0.1.1, https://github.com/lb664/MR2 (2025).
35. Hemani, G., Elsworth, B., Palmer, T. & Rasteiro, *R.* ieugwasr: Interface to the 'OpenGWAS' Database API. R package version 1.1.0, https://CRAN.R-project.org/package=ieugwasr (2025).
36. 1000 Genomes Project Consortium, Auton, A., Brooks, L.D., Durbin, R.M., Garrison, E.P., Kang, H.M., Korbel, J.O., Marchini, J.L., McCarthy, S., McVean, G.A., and Abecasis, G.R. (2015). A global reference for human genetic variation. Nature *526*, 68–74. https://doi.org/10.1038/nature15393.
37. Burgess, S., Dudbridge, F., and Thompson, S.G. (2016). Combining information on multiple instrumental variables in Mendelian randomization: comparison of allele score and summarized data methods. Stat. Med. *35*, 1880–1906. https://doi.org/10.1002/sim.6835.
38. Burgess, S., and Thompson, S.G. (2017). Interpreting findings from Mendelian randomization using the MR-Egger method. Eur. J. Epidemiol. *32*, 377–389. https://doi.org/10.1007/s10654-017-0255-x.
39. Bryois, J., Calini, D., Macnair, W., Foo, L., Urich, E., Ortmann, W., Iglesias, V.A., Selvaraj, S., Nutma, E., Marzin, M., et al. (2022). Cell-type-specific cis-eQTLs in eight human brain cell types identify novel risk genes for psychiatric and neurological disorders. Nat. Neurosci. *25*, 1104–1112. https://doi.org/10.1038/s41593-022-01128-z.
40. Bennett, D.A., Buchman, A.S., Boyle, P.A., Barnes, L.L., Wilson, R.S., and Schneider, J.A. (2018). Religious orders study and rush memory and aging project. J. Alzheimers Dis. *64*, S161–S189. https://doi.org/10.3233/JAD-179939.
41. Mi, H., Muruganujan, A., and Thomas, P.D. (2013). PANTHER in 2013: modeling the evolution of gene function, and other gene attributes, in the context of phylogenetic trees. Nucleic Acids Res. *41*, D377–D386. https://doi.org/10.1093/nar/gks1118.
42. Wegmann, S., Biernat, J., and Mandelkow, E. (2021). A current view on Tau protein phosphorylation in Alzheimer's disease. Curr. Opin. Neurobiol. *69*, 131–138. https://doi.org/10.1016/j.conb.2021.03.003.

43. Wainberg, M., Andrews, S.J., and Tripathy, S.J. (2023). Shared genetic risk loci between Alzheimer's disease and related dementias, Parkinson's disease, and amyotrophic lateral sclerosis. Alzheimers Res. Ther. *15*, 113. https://doi.org/10.1186/s13195-023-01244-3.
44. Koks, S., Pfaff, A.L., Bubb, V.J., and Quinn, J.P. (2021). Transcript variants of genes involved in neurodegeneration are differentially regulated by the APOE and MAPT haplotypes. Genes *12*, 423. https://doi.org/10.3390/genes12030423.
45. Lambert, J.-C., Heath, S., Even, G., Campion, D., Sleegers, K., Hiltunen, M., Combarros, O., Zelenika, D., Bullido, M.J., Tavernier, B., et al. (2009). Genome-wide association study identifies variants at CLU and CR1 associated with Alzheimer's disease. Nat. Genet. *41*, 1094–1099. https://doi.org/10.1038/ng.439.
46. Lunnon, K., Sattlecker, M., Furney, S.J., Coppola, G., Simmons, A., Proitsi, P., Lupton, M.K., Lourdusamy, A., Johnston, C., Soininen, H., et al. (2013). A blood gene expression marker of early Alzheimer's disease. J. Alzheimers Dis. *33*, 737–753. https://doi.org/10.3233/JAD-2012-121363.
47. Fujita, M., Gao, Z., Zeng, L., McCabe, C., White, C.C., Ng, B., Green, G.S., Rozenblatt-Rosen, O., Phillips, D., Amir-Zilberstein, L., et al. (2024). Cell subtype-specific effects of genetic variation in the Alzheimer's disease brain. Nat. Genet. *56*, 605–614. https://doi.org/10.1038/s41588-024-01685-y.
48. GTEx Consortium (2020). The GTEx Consortium atlas of genetic regulatory effects across human tissues. Science *369*, 1318–1330. https://doi.org/10.1126/science.aaz1776.
49. Li, M., Hao, X., Hu, Z., Tian, J., Shi, J., Ma, D., Guo, M., Li, S., Zuo, C., Liang, Y., et al. (2024). Microvascular and cellular dysfunctions in Alzheimer's disease: An integrative analysis perspective. Sci. Rep. *14*, 20944. https://doi.org/10.1038/s41598-024-71888-0.
50. Hu, Q., Zhang, X., Huang, J., Peng, H., Sun, Y., Sang, W., Jiang, B., and Sun, D. (2024). The STAT1-SLC31A1 axis: Potential regulation of cuproptosis in diabetic retinopathy. Gene *930*, 148861. https://doi.org/10.1016/j.gene.2024.148861.
51. Nakagawa, Y., and Yamada, S. (2023). The relationships among metal homeostasis, mitochondria, and locus coeruleus in psychiatric and neurodegenerative disorders: Potential pathogenetic mechanism and therapeutic implications. Cell. Mol. Neurobiol. *43*, 963–989. https://doi.org/10.1007/s10571-022-01234-3.
52. Li, L., Huang, K.-L., Gao, Y., Cui, Y., Wang, G., Elrod, N.D., Li, Y., Chen, Y.E., Ji, P., Peng, F., et al. (2021). An atlas of alternative polyadenylation quantitative trait loci contributing to complex trait and disease heritability. Nat. Genet. *53*, 994–1005. https://doi.org/10.1038/s41588-021-00864-5.
53. Cui, Y., Peng, F., Wang, D., Li, Y., Li, J.S., Li, L., and Li, W. (2022). 3'aQTL-atlas: an atlas of 3'UTR alternative polyadenylation quantitative trait loci across human normal tissues. Nucleic Acids Res. *50*, D39–D45. https://doi.org/10.1093/nar/gkab740.
54. Kang, B., Yang, Y., Hu, K., Ruan, X., Liu, Y.-L., Lee, P., Lee, J., Wang, J., and Zhang, X. (2023). Infernape uncovers cell type–specific and spatially resolved alternative polyadenylation in the brain. Genome Res. *33*, 1774–1787. https://doi.org/10.1101/gr.277864.123.
55. Mittleman, B.E., Pott, S., Warland, S., Zeng, T., Mu, Z., Kaur, M., Gilad, Y., and Li, Y. (2020). Alternative polyadenylation mediates genetic regulation of gene expression. eLife *9*, e57492. https://doi.org/10.7554/eLife.57492.
56. Cao, J., and Kuyumcu-Martinez, M.N. (2023). Alternative polyadenylation regulation in cardiac development and cardiovascular disease. Cardiovasc. Res. *119*, 1324–1335. https://doi.org/10.1093/cvr/cvad014.
57. Roselli, C., Chaffin, M.D., Weng, L.-C., Aeschbacher, S., Ahlberg, G., Albert, C.M., Almgren, P., Alonso, A., Anderson, C.D., Aragam, K.G., et al. (2018). Multi-ethnic genome-wide association study for atrial fibrillation. Nat. Genet. *50*, 1225–1233. https://doi.org/10.1038/s41588-018-0133-9.
58. Migdady, I., Russman, A., and Buletko, A.B. (2021). Atrial fibrillation and ischemic stroke: a clinical review. Semin. Neurol. *41*, 348–364. Thieme Medical Publishers, Inc. https://doi.org/10.1055/s-0041-1726332.
59. Dulli, D.A., Stanko, H., and Levine, R.L. (2003). Atrial fibrillation is associated with severe acute ischemic stroke. Neuroepidemiology *22*, 118–123. https://doi.org/10.1159/000068743.
60. Marini, C., De Santis, F., Sacco, S., Russo, T., Olivieri, L., Totaro, R., and Carolei, A. (2005). Contribution of atrial fibrillation to incidence and outcome of ischemic stroke: results from a population-based study. Stroke *36*, 1115–1119. https://doi.org/10.1161/01.STR.0000166053.83476.4a.
61. Friberg, L., Rosenqvist, M., Lindgren, A., Terént, A., Norrving, B., and Asplund, K. (2014). High prevalence of atrial fibrillation among patients with ischemic stroke. Stroke *45*, 2599–2605. https://doi.org/10.1161/STROKEAHA.114.006070.
62. Frerich, S., Malik, R., Georgakis, M.K., Sinner, M.F., Kittner, S.J., Mitchell, B.D., and Dichgans, M. (2022). Cardiac risk factors for stroke: a comprehensive Mendelian randomization study. Stroke *53*, e130–e135. https://doi.org/10.1161/STROKEAHA.121.036306.
63. Georgakis, M.K., Malik, R., Gill, D., Franceschini, N., Sudlow, C.L.M., Dichgans, M.; and INVENT Consortium,CHARGE Inflammation Working Group (2020). Interleukin-6 signaling effects on ischemic stroke and other cardiovascular outcomes: a Mendelian randomization study. Circ. Genom. Precis. Med. *13*, e002872. https://doi.org/10.1161/CIRCGEN.119.002872.
64. Wang, Q., Richardson, T.G., Sanderson, E., Tudball, M.J., Ala-Korpela, M., Davey Smith, G., and Holmes, M.V. (2022). A phenome-wide bidirectional Mendelian randomization analysis of atrial fibrillation. Int. J. Epidemiol. *51*, 1153–1166. https://doi.org/10.1093/ije/dyac041.
65. Hou, L., Xu, M., Yu, Y., Sun, X., Liu, X., Liu, L., Li, Y., Yuan, T., Li, W., Li, H., and Xue, F. (2020). Exploring the causal pathway from ischemic stroke to atrial fibrillation: a network Mendelian randomization study. Mol. Med. *26*, 7–9. https://doi.org/10.1186/s10020-019-0133-y.
66. Yao, P., Mazidi, M., Pozarickij, A., Iona, A., Wright, N., Lin, K., Millwood, I.Y., Fry, H., Kartsonaki, C., Chen, Y., et al. (2025). Proteome-Wide Genetic Study in East Asians and Europeans Identified Multiple Therapeutic Targets for Ischemic Stroke. Stroke *56*, 2147–2158. https://doi.org/10.1161/STROKEAHA.125.050982.
67. Feng, X., Li, L., Wagner, E.J., and Li, W. (2018). TC3A: the cancer 3′ UTR atlas. Nucleic Acids Res. *46*, D1027–D1030. https://doi.org/10.1093/nar/gkx892.
68. Mishra, A., Malik, R., Hachiya, T., Jürgenson, T., Namba, S., Posner, D.C., Kamanu, F.K., Koido, M., Le Grand, Q., Shi, M., et al. (2022). Stroke genetics informs drug discovery and risk prediction across ancestries. Nature *611*, 115–123. https://doi.org/10.1038/s41586-022-05165-3.

69. Nielsen, J.B., Thorolfsdottir, R.B., Fritsche, L.G., Zhou, W., Skov, M.W., Graham, S.E., Herron, T.J., McCarthy, S., Schmidt, E.M., Sveinbjornsson, G., et al. (2018). Biobank-driven genomic discovery yields new insight into atrial fibrillation biology. Nat. Genet. *50*, 1234–1239. https://doi.org/10.1038/s41588-018-0171-3.
70. Wang, R., Nambiar, R., Zheng, D., and Tian, B. (2018). PolyA_DB 3 catalogs cleavage and polyadenylation sites identified by deep sequencing in multiple genomes. Nucleic Acids Res. *46*, D315–D319. https://doi.org/10.1093/nar/gkx1000.
71. Ogorodnikov, A., and Danckwardt, S. (2021). TRENDseq—a highly multiplexed high throughput RNA 3′ end sequencing for mapping alternative polyadenylation. Methods Enzymol. *655*, 37–72. https://doi.org/10.1016/bs.mie.2021.03.022.
72. Müller, S., Rycak, L., Afonso-Grunz, F., Winter, P., Zawada, A.M., Damrath, E., Scheider, J., Schmäh, J., Koch, I., Kahl, G., and Rotter, B. (2014). APADB: a database for alternative polyadenylation and microRNA regulation events. Database *2014*, bau076. https://doi.org/10.1093/database/bau076.
73. Braunersreuther, V., Montecucco, F., Asrih, M., Pelli, G., Galan, K., Frias, M., Burger, F., Quinderé, A.L.G., Montessuit, C., Krause, K.-H., et al. (2013). Role of NADPH oxidase isoforms NOX1, NOX2 and NOX4 in myocardial ischemia/reperfusion injury. J. Mol. Cell. Cardiol. *64*, 99–107. https://doi.org/10.1016/j.yjmcc.2013.09.007.
74. Youn, J.-Y., Zhang, J., Zhang, Y., Chen, H., Liu, D., Ping, P., Weiss, J.N., and Cai, H. (2013). Oxidative stress in atrial fibrillation: an emerging role of NADPH oxidase. J. Mol. Cell. Cardiol. *62*, 72–79. https://doi.org/10.1016/j.yjmcc.2013.04.019.
75. Wang, Y., Qu, H., and Liu, J. (2020). P66Shc deletion ameliorates oxidative stress and cardiac dysfunction in pressure overload-induced heart failure. J. Card. Fail. *26*, 243–253. https://doi.org/10.1016/j.cardfail.2019.09.003.
76. Haslem, L., Hays, J.M., and Hays, F.A. (2022). p66Shc in cardiovascular pathology. Cells *11*, 1855. https://doi.org/10.3390/cells11111855.
77. Roselli, C., Surakka, I., Olesen, M.S., Sveinbjornsson, G., Marston, N.A., Choi, S.H., Holm, H., Chaffin, M., Gudbjartsson, D., Hill, M.C., et al. (2025). Meta-analysis of genome-wide associations and polygenic risk prediction for atrial fibrillation in more than 180,000 cases. Nat. Genet. *57*, 539–547. https://doi.org/10.1038/s41588-024-02072-3.
78. Woodcock, E.A., Kistler, P.M., and Ju, Y.-K. (2009). Phosphoinositide signalling and cardiac arrhythmias. Cardiovasc. Res. *82*, 286–295. https://doi.org/10.1093/cvr/cvn283.
79. Heijman, J., Voigt, N., Nattel, S., and Dobrev, D. (2014). Cellular and molecular electrophysiology of atrial fibrillation initiation, maintenance, and progression. Circ. Res. *114*, 1483–1499. https://doi.org/10.1161/CIRCRESAHA.114.302226.
80. Zhang, Y., Pletcher, M.J., Vittinghoff, E., Clemons, A.M., Jacobs, D.R., Allen, N.B., Alonso, A., Bellows, B.K., Oelsner, E.C., Zeki Al Hazzouri, A., et al. (2021). Association between cumulative low-density lipoprotein cholesterol exposure during young adulthood and middle age and risk of cardiovascular events. JAMA Cardiol. *6*, 1406–1413. https://doi.org/10.1001/jamacardio.2021.3508.
81. Hou, X., Zheng, J., Zhang, J., Tao, L., Cen, K., Cui, Y., and Wu, J. (2024). Evaluating the Causal Effects of Low Density Lipoprotein Cholesterol Levels on Ischemic Stroke: A Mendelian Randomization Study. Iran. J. Public Health *53*, 397–403. https://doi.org/10.18502/ijph.v53i2.14924.
82. Hindy, G., Engström, G., Larsson, S.C., Traylor, M., Markus, H.S., Melander, O., Orho-Melander, M.; and Stroke Genetics Network SiGN (2018). Role of blood lipids in the development of ischemic stroke and its subtypes: a Mendelian randomization study. Stroke *49*, 820–827. https://doi.org/10.1161/STROKEAHA.117.019653.
83. Ference, B.A., Ginsberg, H.N., Graham, I., Ray, K.K., Packard, C.J., Bruckert, E., Hegele, R.A., Krauss, R.M., Raal, F.J., Schunkert, H., et al. (2017). Low-density lipoproteins cause atherosclerotic cardiovascular disease. 1. Evidence from genetic, epidemiologic, and clinical studies. A consensus statement from the European Atherosclerosis Society Consensus Panel. Eur. Heart J. *38*, 2459–2472. https://doi.org/10.1093/eurheartj/ehx144.
84. Sabatine, M.S., Giugliano, R.P., Keech, A., Honarpour, N., Wang, H., Liu, T., Wasserman, S.M., Scott, R., Sever, P.S., and Pedersen, T.R. (2016). Rationale and design of the Further cardiovascular OUtcomes Research with PCSK9 Inhibition in subjects with Elevated Risk trial. Am. Heart J. *173*, 94–101. https://doi.org/10.1016/j.ahj.2015.11.015.
85. Wu, S., Smith, A., Huang, J., Otto, G.W., Ko, Y.-H., Yarmolinsky, J., Gill, D., Rohatgi, A., Dehghan, A., Tzoulaki, I., and Meena, D. (2024). Prioritizing protein targets for dyslipidaemia and cardiovascular diseases using Mendelian randomization in South Asians. medRxiv. https://doi.org/10.1101/2024.12.18.24319223.
86. Ken-Dror, G., Ajami, I., Han, T.S., Aurelius, T., Maheshwari, A., Hail, H.A., Deleu, D., Sharma, S.D., Amlani, S., Gunathilagan, G., et al. (2024). Diabetes mellitus and obesity among South Asians with ischemic stroke across three countries. Int. J. Stroke *19*, 235–243. https://doi.org/10.1177/17474930231203149.
87. Eastwood, S.V., Tillin, T., Chaturvedi, N., and Hughes, A.D. (2015). Ethnic differences in associations between blood pressure and stroke in South Asian and European men. Hypertension *66*, 481–488. https://doi.org/10.1161/HYPERTENSIONAHA.115.05672.
88. Graham, S.E., Clarke, S.L., Wu, K.-H.H., Kanoni, S., Zajac, G.J.M., Ramdas, S., Surakka, I., Ntalla, I., Vedantam, S., Winkler, T.W., et al. (2021). The power of genetic diversity in genome-wide association studies of lipids. Nature *600*, 675–679. https://doi.org/10.1038/s41586-021-04064-3.